

Landslide assessment using interferometric synthetic aperture radar in Pacitan, East Java

Dimas Bayu Ichсандya, Muhammad Dimiyati, Iqbal Putut Ash Shidiq, Faris Zulkarnain, Nurul Sri Rahatiningtyas, Riza Putera Syamsuddin, Farhan Makarim Zein

Department of Geography, Faculty of Mathematics and Natural Sciences, Universitas Indonesia, Depok City, Indonesia

Article Info

Article history:

Received Jun 6, 2021

Revised Dec 16, 2021

Accepted Jan 2, 2022

Keywords:

Depletion zone

InSAR

Landslide

LiCSBAS

Surface deformation

ABSTRACT

Landslides are a common type of disaster in Indonesia, especially in steep-slope areas. The landslide process can be well understood by measuring the surface deformation. Currently, there are no practical solutions for measuring surface deformation at landslide locations other than field surveys in the Pacitan Regency. We apply LiCSBAS, to identify surface deformation in several landslide locations in a specific non-urban area with mixed topographical features. LiCSBAS is a module that utilizes data from the project of looking inside the continent from space (LiCS), using the new small baseline area subset (NSBAS) method. This study utilizes the leaf area index (LAI) to validate the ability of LiCSBAS to detect surface deformation values at landslide locations. The study succeeded in identifying surface deformations at 100 landslide locations, with deformation values ranging from 15.1 to 10.9 millimeters per year. Most of the landslide locations are closely related to volcanic rocks and volcanic sediments on slopes of 30–35°. The NSBAS method in the LiCSBAS module can reduce gaps error in the sentinel-1 image network. However, the utilization of the C-band at a pixel size of 100 meters made surface deformation only well detectable in a large open landslide area.

This is an open access article under the [CC BY-SA](https://creativecommons.org/licenses/by-sa/4.0/) license.



Corresponding Author:

Muhammad Dimiyati

Department of Geography, Faculty of Mathematics and Natural Sciences, Universitas Indonesia

Margonda Raya Street, Pondok Cina, Beji, Depok City, East Java, Indonesia

Email: m.dimiyati@sci.ui.ac.id

1. INTRODUCTION

Soil surface deformation is a dynamic process on the earth's surface [1]. This process occurs naturally or due to human intervention [2]. One form of such deformation is a landslide. Landslide is a mass movement of soil or rock on the disrupted slope [3]. Landslides have caused casualties and material losses in many countries [4]. Pacitan Regency is the area with the highest number of landslide occurrences in East Java Province. The worst landslide events occurred in 2017, along with the Cempaka tropical cyclone; more than 210 landslides were causing 19 deaths, destroying 615 houses, and causing loss of more than 615 billion rupiahs [5]. Therefore, strategic planning to reduce losses and casualties is necessarily conducted through data inventory (mapping) and ground movements identification [6]–[9].

Methods for detecting and monitoring ground movements are continuously evolving using remote sensing imagery, both optical and synthetic aperture radar (SAR) and field measurement data [2]. Some advantages of using satellite monitoring include having a large coverage area, immediate data acquisition, and ultimately reducing operational costs. One of them is using differential interferometry synthetic aperture radar (DInSAR). DInSAR works by utilizing different phases of SAR images in the same area at different times [10]. The use of DInSAR for the detection and monitoring of ground motion includes the persistent scatterer

interferometry synthetic aperture radar (PSInSAR) and small baseline area subset (SBAS) method [2], [11]–[15]. PSInSAR works using a single master interferogram to form persistent scatterer (PS) [16]. Meanwhile, SBAS works by utilizing multiple master interferograms with smaller temporal and spatial baselines [17]. The study of surface deformation in non-urban areas usually uses the SBAS method by utilizing several master interferograms [12], [14], [18]. Moreover, SBAS does not depend on PS density to evaluate surface deformation [18]. However, the SBAS method uses large amounts of data and requires compatible devices for processing on a long temporal scale and regional-level analysis. To overcome these limitations, users can use LiCSBAS, an open-source InSAR multi-temporal analysis module [19]–[21]. LiCSBAS utilizes sentinel-1 SAR data that LiCSAR has processed, so users do not need to download enormous datasets on their computers [20]. LiCSBAS uses the Python3 and the bourne again shell (Bash) to write commands. LiCSBAS allowed us to measure surface deformation at a millimeter-scale [19].

The current use of LiCSBAS focuses on large-scale surface deformation in tectonic and volcanic studies [21]. LiCSBAS, on the other hand, has the potential to be used in hydrosphere, cryosphere, and mass movement studies [20]. Unfortunately, there are no practical solutions for addressing surface deformation in landslide locations with various physical and environmental conditions other than field surveys. Another challenging issue is related to the implementation of LiCSBAS in a non-urban area with different lithological and topographical characteristics. Therefore, this study aims to implement the LiCSBAS module on a multi-temporal InSAR to detect surface deformation values at landslides locations in the Pacitan Regency, which has the characteristics described above. This study also utilizes overlay analysis to determine the distribution of landslide locations based on lithological formations and slopes. In addition, this study uses the Leaf Area Index (LAI) to determine the vegetation dynamics that can affect the coherence of the interferogram.

2. RESEARCH METHOD

2.1. Study area

The study area of Pacitan Regency, East Java Province, Indonesia, consists of 12 sub-districts with about 1,417 km² and occupied by 586,110 people in 2020 [22]. Land-use/land-cover data from the Indonesian geospatial information agency (BIG) shows that the Pacitan Regency is dominated by shrubs, covering more than 36,000 hectares. In contrast, others types are dryland farming (31,444 hectares), mixed plantations (18,540 hectares), rainfed rice fields (18,540 hectares), and settlement areas (15,031 hectares) [23]. This study used 358 landslide locations. As many as 258 landslide locations are the data from the regional disaster management agency (BPBD) of Pacitan Regency inventory in 2017–2020. The remaining 100 landslide locations are the results of identification through field surveys and interpretation of high-resolution Airbus and the Centre National d'Etudes Spatiales (CNES) imagery in 2017–2020 accessed via Google Earth.

Hilly topography dominates the study area, which is also part of the Southern Mountains [24]. The downstream of the Grindulu River and the Lorok River have a relatively flat topography. Table 1 shows the results of slope classification in Pacitan Regency. The central part of the Pacitan Regency has a steeper slope compared to the southern part. However, as indicated in Figure 1, numerous high-degree slopes were also found in the south-eastern part of the area, particularly in the northern part of the Ngadirojo Sub-District. The Arjosari Formation is the widest, and the Kalipucang Formation is the narrowest, according to the area of each lithological formation as shown in Figure 2 and Table 2.

Table 1. Percentage areas of slope classes

No	Slope	Area (hectares)	(percent)
1	0-5°	13,250	9.3
2	5-10°	25,755	18.1
3	10-15°	30,399	21.4
4	15-20°	27,744	19.5
5	20-25°	21,056	14.8
6	25-30°	13,573	9.5
7	>30°	9,951	7

Source: Calculated from Digital Elevation Model-National (DEMNAS) [25] based on [26]

On the other hand, leaf area index (LAI) indicates the density of plant canopy in a particular area and is usually defined in m² [27], [28]. Figure 3 illustrates the average value of LAI in the Pacitan Regency from 2017–2020 predicted from sentinel-2A Multi Spectral Instrument (MSI) imagery processed using the Google Earth Engine (GEE). The lowest LAI values are illustrated as red-colored zones along the Grindulu River and the Lorok Rivers, indicating sedimentary material and sparse vegetation cover. Meanwhile, high LAI values

are illustrated as blue-colored zones in the central and eastern parts of the Pacitan Regency with hilly topography and covered with agricultural and non-agricultural vegetation.

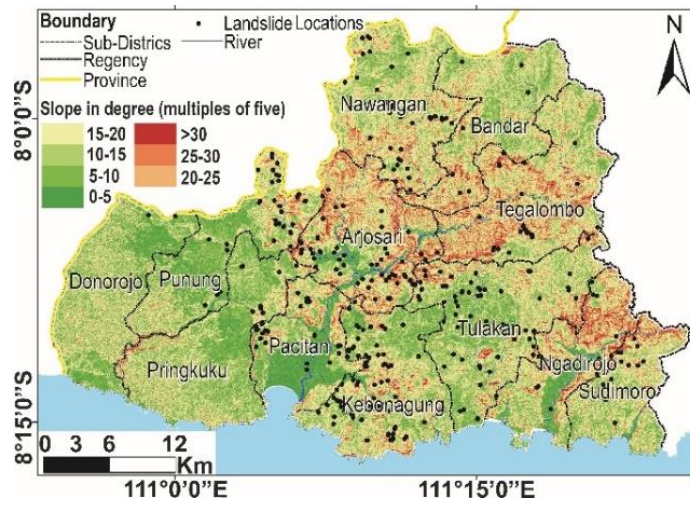


Figure 1. Slope class distribution in Pacitan Regency, calculated from DEMNAS [25] based on [26]

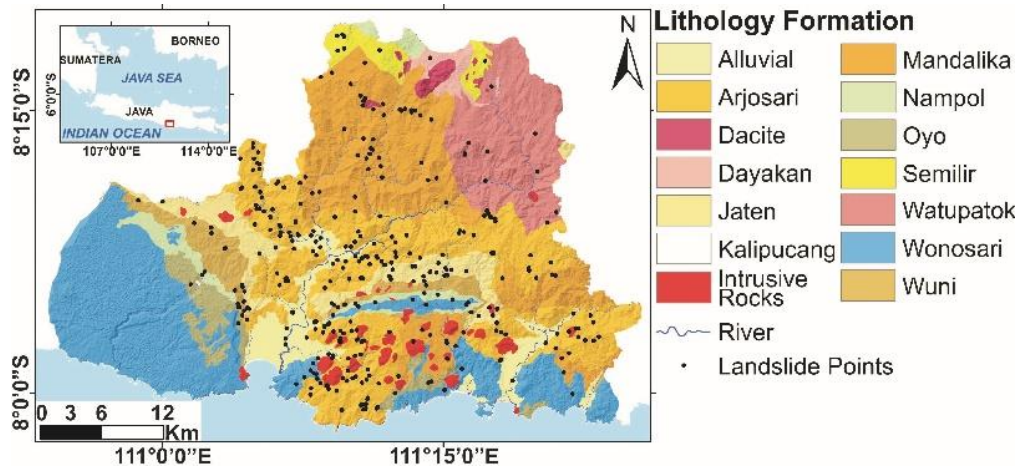


Figure 2. Lithological formations in Pacitan Regency [29], [30]

Table 2. Distribution of rock formation

No	Formation	Rock materials	Area (hectares)	Area (%)
1	Alluvial	alluvium	7,397	5.2
2	Arjosari	polymictic breccias, sandstone, and conglomerates alternating with volcanic rock	33,150	23.3
3	Dacite	dacite, alluvium, and another intrusive rock	1,101	0.7
4	Dayakan	sandstone and claystone	1,543	1
5	Intrusive Rock	intrusive rock	3,250	2.2
6	Jaten	conglomerate, sandstone, mudstone, lignite, shale, and tuff	7,743	5.4
7	Kalipucang	conglomerates and clay	18	0.01
8	Mandalika	volcanic breccias and lava tuffs altering with sandstone and siltstone	26,273	18.5
9	Nampol	sandstone, siltstone, limestone, and lignite with conglomerate and breccia	3,624	2.5
10	Oyo	sandstone, siltstone, limestone, and marl	4,466	3.1
11	Semilir	tuff, sandstone breccia, and siltstone	2,974	2
12	Watupatok	basalt pillow lava, sandstone, claystone, and chert	14,676	10.3
13	Wonosari	reef limestone, limestone deposits, sandy limestone, and marl	30,114	21.2
14	Wuni	volcanic breccias, tuffs, and sandstone alternating with lignite and limestone	5,380	3.7

Source: Lithological formations of Pacitan Regency [29], [30]

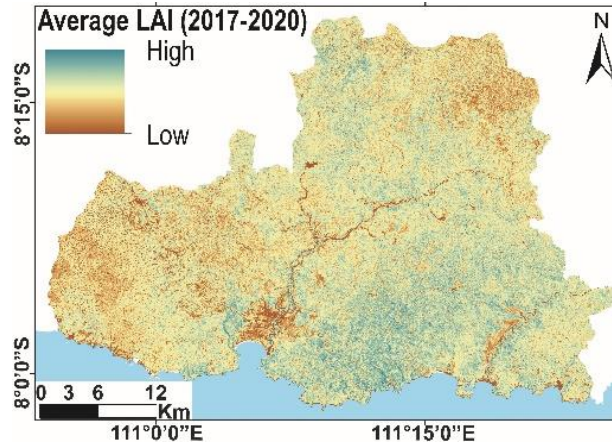


Figure 3. Average LAI from 2017 to 2020, calculated from sentinel-2A multi spectral instrument (MSI) imagery [31]

2.2. Method of SAR data processing

The LiCSBAS module utilizes the LiCSAR product, so users do not need to create interferograms from SLC data on the local computer [19]. This study utilizes 190 Sentinel-1 images of ascending Interferometric Wide, single look complex, and vertical-vertical polarisation (IW SLC VV). The images are automatically processed in LiCSAR to form 812 interferograms with a resolution of 0.0001 or 100 meters [19], [20]. The 190 sentinel-1 images have a 3.24-year observation period, starting from 07-05-2017 and terminating on 01-08-2020, corresponding to the period included in the landslide data inventory. LiCSBAS, coded in python and bourne again shell (bash), was conducted in this study using Ubuntu 20.04 long term support (LTS) software [19]. In general, there are two categories of data processing: data preparation and multi-temporal analysis [19]. In the research [19], [20] for detailed data processing procedures. First, download unwrapped phase and coherence GeoTIFF data from the Centre for the Observation and Modelling of Earthquakes, Volcanoes and Tectonics (COMET)-LiCS website, www.comet.nerc.ac.uk [19]. Second, convert geographic tagged image file format (GeoTIFF) files to a single-precision floating-point format, then used the generic atmospheric correction online service (GACOS) for InSAR data to correct tropospheric noise [19]. Furthermore, mask the de-correlated parts of the interferogram where the phase noise coherence estimates are 0.5 [19], and clip the rectangular area of interest at -7.89° (North), -8.28° (South), 110.90° (West), 111.46° (East).

There are four stages of multi-temporal analysis. First, identify the interferograms based on coherence and unwrapped data coverage that may experience spatial and temporal de-correlation. The next step is by checking the loop closure phase to remove interferograms with many unwrapping errors [19]. The (1) describes the loop closure [32]. ϕ_1, ϕ_2, ϕ_3 are images, and $\phi_{12}, \phi_{23}, \phi_{13}$ are the unwrapped interferograms. The loop phase usually has a value close to zero if there is no unwrapping error in the three interferograms [19];

$$\phi_{123} = \phi_{12} + \phi_{23} - \phi_{13} \tag{1}$$

Second, to obtain the time-series velocity displacement as line of sight (LOS) displacement, invert the stack of unwrapped data [19]. According to [19] and [33], the time series velocity calculation utilizes the NSBAS method by inverting the interferogram network, as shown in (3). The NSBAS technique is a modification of the Small Baseline approach in (2) to overcome the limitation of a time gap on the network [19], [34].

$$d = Gm \tag{2}$$

$$\begin{bmatrix} \mathbf{d} \\ 0 \end{bmatrix} = \gamma \begin{bmatrix} \mathbf{G} & \mathbf{0} & \mathbf{0} \\ 1 & 0 & \dots & \dots & 0 & -t_1 & -1 \\ \vdots & \ddots & \ddots & & \dots & -t_2 & \vdots \\ 1 & \dots & 1 & \ddots & \dots & \vdots & \vdots \\ \vdots & & \vdots & \ddots & 0 & \vdots & \vdots \\ 1 & \dots & 1 & \dots & 1 & -t_{N-1} & -1 \end{bmatrix} \begin{bmatrix} \mathbf{m} \\ v \\ c \end{bmatrix} \tag{3}$$

Third, calculate the standard deviation of the velocity, mask the noisy pixels, and filter the time series velocity [19]. Fourth, calculate and visualize the value of surface deformation at each landslide location. The surface deformation value or LOS displacement value obtained from the interferogram is the result of measuring the movement between the radar antenna and a location on the earth's surface [15]. This value is represented by a size of 100 by 100 meter pixels resolution.

3. RESULTS AND DISCUSSION

3.1. Surface deformation at landslide locations

Surface displacement in the study area varies from -34 to 25 millimeters per year in an area of 33,831 hectares, or 23.8 percent of the Pacitan Regency. As illustrated in Figure 4, the type of deformation observed was subsidence and uplift, covering 10,062 hectares (7.1%) and 23,768 hectares (16.7%), respectively. The most extensive deformation was found in the agricultural and bare-land areas, totaling 21,272 hectares, followed by a built-up area (7,457 hectares) and non-cultivated land (4,367 hectares).

Of the 358 landslide locations, 46 landslide locations have negative displacement values ranging from 15.1 millimeters per year to 0.05 millimeters per year. On the other hand, 54 landslide locations had positive displacement values ranging from 0.3 to 10.9 millimeters per year. Meanwhile, the displacement value at 258 landslide locations remains undetected. This undetected displacement at landslide locations is associated with a small landslide area covered with vegetation, as shown in Figure 5.

Surface deformation is undetected in most areas of the Pacitan Regency due to the low coherence values found in several areas. This circumstance might be related to the geometric distortion effect due to the side-looking direction of the image acquisition in the SAR system [35]. For example, the shadow can occur when hills block the radar beam so that the sensor receives no backscatter from the object, which is characterized by dark areas in the coherence image [36]. Furthermore, dense vegetation might cause the backscatter to be weaker, reducing the coherence value in the interferogram [21]. Therefore, the LiCSBAS module will automatically mask pixels with a coherence value of less than 0.5 [19].

High hilly areas covered with hardwood trees and dense canopy in the central part of the Pacitan Regency have low density of surface deformation pixel. The dominance of high LAI values indicates this circumstance. Figure 4 shows the distribution and pixel values of the surface deformation. The built-up region (in the red box) has a high surface deformation pixel density because the C-band SAR signal produces a high coherence value. The red boxes on the west and east sides represent the downstream of the Grindulu River in the Pacitan Sub-District and the downstream of the Lorok River in Ngadirojo Sub-District, respectively. In the west part of the Pacitan Regency, in the Sub-Districts of Donorojo, Punung, and Pringkuku, medium-density deformation pixels may be detected. Most of this area is open land with sparse vegetation.

The spatial information of landslide zones is essential to analyze the LOS displacement value. For this purpose, landslides can be divided into depletion and accumulation zone [2], [37]. The depletion zone is a source of landslides characterized by a scarp at the top of the landslide [2], [26]. The accumulation zone is considered the fill zone of landslide material from the depletion zone [37]. The depletion zone has a negative LOS displacement value because the distance between a point on the earth's surface and the satellite radar sensor gets further away and vice versa in the accumulation zone [38].

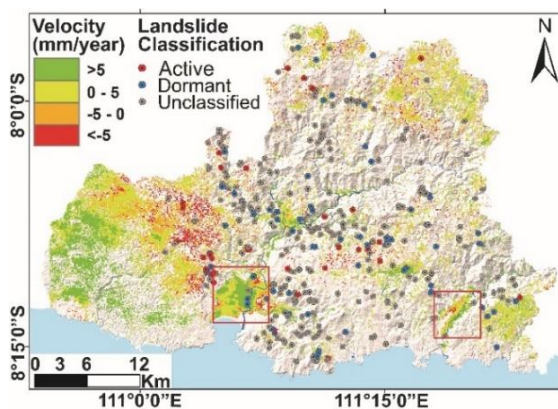


Figure 4. Distributions of surface deformation velocity pixels and landslide locations classification based on LOS displacement values, data processed from [39] based on [19]



Figure 5. Small landslides on the side of the road in Bubakan Village, Tulakan Sub-District

Figures 6 illustrates three landslide locations whose deformation from LOS displacement values were detected, both in the depletion and accumulation zones or one of them. The delineation lines on the scarp, depletion, and accumulation zones result from field surveys and identification of satellite images. The three landslide locations are included in the Arjosari and Mandalika Formation, with a slope class of 10-20°, each area of more than 1 hectare. Figure 6(a) is a landslide in Kalikuning Village, Tulakan Sub-District, with an elevation at point of interest (POI) 1 of 336 meters. POI 1 is located at the bottom of the landslide or accumulation zone, evidenced by a positive LOS displacement value of 9.4 millimeters per year. Figure 6(b) is a landslide in Kedungbendo Village, Arjosari Sub-District, with an elevation of POI 2 of 57 meters and POI 3 of 245 meters. POI 2 is located in the accumulation zone, evidenced by a positive LOS displacement value of 8.8 millimeters per year. POI 3 is located in the depletion zone, with a negative LOS displacement value of -5.1 millimeters per year. Figure 6(c) is a landslide in Ponggok Village, Pacitan Sub-District, with an elevation at POI 4 of 345 meters. POI 4 is located in the depletion zone, evidenced by a negative LOS displacement value of -9.8 millimeters per year.

In Figure 7, the LOS displacement time-series at each POI shows a trend indicating surface deformation still happens at landslide locations during the study period. In Figures 7(a) and 7(b), the trend line at POI 1 and POI 2 has an increasing trend with a positive average LOS displacement. The positive LOS displacement value indicates that the distance between the earth's surface and the satellite sensor is getting closer due to the increasing pile of material from the depletion zone. The opposite occurs in Figures 7(c) and 7(d), where the average LOS displacement values at POI 3 and POI 4 are decreasing, which indicates the distance between the earth's surface and the satellite sensor is getting farther away caused by the decrease in slope materials towards the accumulation zone.

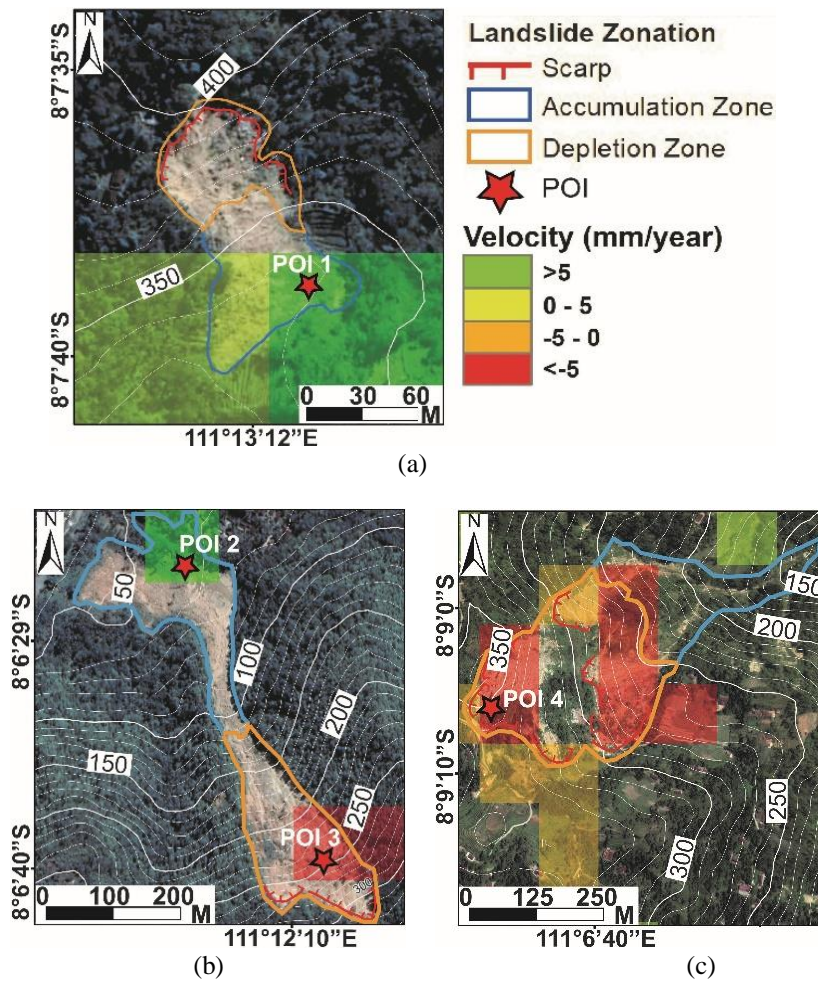


Figure 6. Detected LOS displacement at landslide zone and point of interest locations (a) detected accumulation zone in Kalikuning Village, Tulakan Sub-District, (b) detected depletion and accumulation zone in Kedungbendo Village, Arjosari Sub-District, and (c) detected depletion and accumulation zone in Ponggok Village, Pacitan Sub-District

In order to classify the activeness of landslides based on their surface deformation values, this study uses a threshold with a value of LOS displacement of 1.5 millimeters per year. According to [12], landslides are considered moving or active when at least one displacement pixel is in the landslide location with a value of LOS displacement of less than -1.5 or more than 1.5 millimeters per year. The NSBAS technique in the LiCSBAS module can identify the LOS displacement values at 100 landslide locations in Pacitan Regency. Of the 74 landslide locations that are still active, it consists of 30 landslide locations with negative displacement values between -1.5 and 15.1 millimeters per year and 44 other locations with positive values of 1.5 to 10.9 millimeters per year. The other 258 locations could not be classified because the displacement values were not detected. According to [12], this is due to the low coherence value in most areas because of vegetation cover and shadow errors in hilly areas.

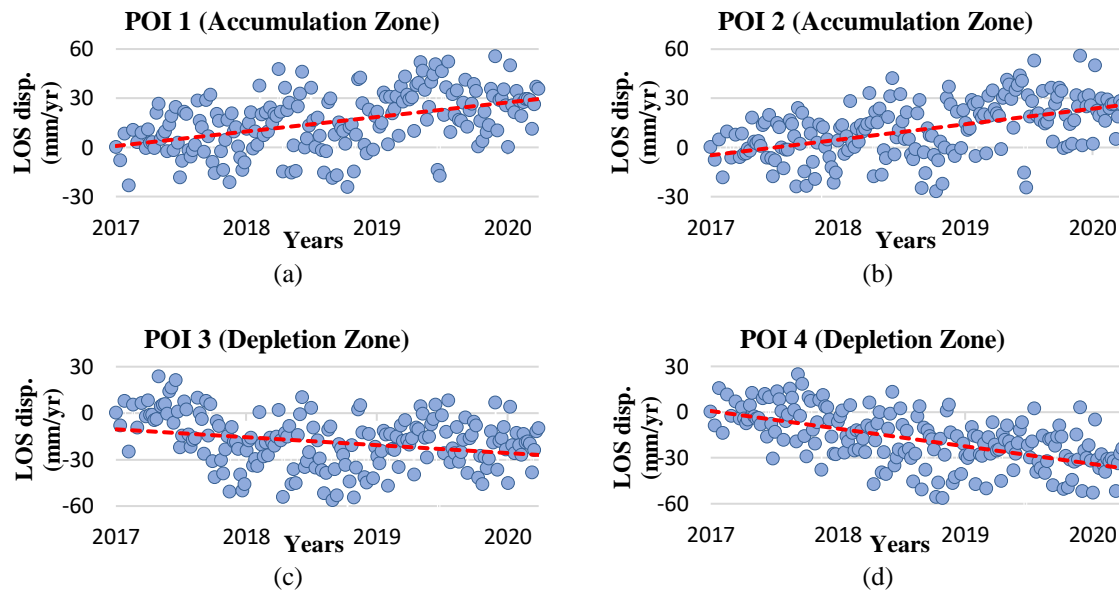


Figure 7. LOS displacement time-series for selected point of interest at the accumulation zone (a) POI 1, (b) POI 2; and at the depletion zone, (c) POI 3, and (d) POI 4

3.2. Distribution of landslide locations based on lithological formations and slopes

The overlay analysis between the geological map sheets of Pacitan and Ponorogo with the landslide location shows that the Arjosari formation has the highest number of landslide occurrences (191 locations; 45 percent), followed by Mandalika formation (53 locations; 18.5 percent) and Jaten formation (36 locations; 10 percent) as shown in Figure 8(a). The three rock formations are volcanic rock and old volcanic sediments that form steep slopes and dominate, especially in the eastern part of the Pacitan Regency [40]. These sedimentary rocks have a quickly loose and weathered structure; therefore, they have higher landslide susceptibility [41].

The formations with the least number of landslide occurrences are Wonosari (17 locations; 4.7 percent), Intrusive Rock (16 locations; 4.4 percent), Wuni (14 locations; 3.9 percent), Nampol (12 locations; 3.3 percent), Watupatok (11 locations; 3 percent), Semilir and Oyo (7 locations; 1.9 percent), Dacite and Dayakan (1 point; 0.2 percent). Meanwhile, there was no landslide during 2017-2020 recorded in the Kalipucang formation. Only a few landslides appeared in the western part of the Pacitan Regency, where the Wonosari Formation dominates. This formation forms low labyrinth-cone karst due to limestone weathering [40], [42]. Although the Wonosari formation occupies 30,114 hectares or 21.2 percent overall, only 17 landslide locations or 4.7 percent are associated with it, which means that the Wonosari Formation has lower landslide susceptibility.

Based on the overlay results, it is known that most of the landslide's location at 15-30, as shown in Figure 8(b). In more detail, the most landslide locations were found in the slope class 15-20 (82 locations; 23 percent), followed by the slope class 20-25 (76 locations; 21%), class 25-30 (61 locations; 17%), class 10-15 (53 locations; 14%), class 5-10° (37 locations; 10%), class 30-35° (25 locations; 7%), class 25-40 (12 locations; 3%), class 0-5 (10 locations; 3 %), and class 40-45 (2 locations; 0.5%).

Based on the overlay between the slopes and the landslide locations, most of the landslides were recorded in the 15-20 slope class of 83 locations or 22.9 percent, followed by the 20-25 slope class of 76 locations or 21.2 percent, and the 25-30° slope class of 61 locations or 17 percent. Based on Figure 8(b), the frequency of landslide locations increases until the slope class of 15-20, then decreases as the slope class increases. According to [43]–[45], the decrease in the number of landslides after the 15-20 slope class has a relationship with the high rate of erosion along with the increase in the slope value. As a result, the soil material cannot thicken, and stable hard rock is exposed. Meanwhile, erosion on riverbanks causes landslides on slopes of 0-5.

Apart from natural conditions, human activities are also influencing landslide occurrences [46]. For example, surface modification by cutting slopes for road and house construction can reduce soil shear resistance; therefore, it cannot maintain slope stability under saturated conditions [47], [48]. As a result, The shear strength on the slope will increase while the resisting strength will decrease, thereby increasing the landslide probability [48].

Land cover type might also affect the occurrence of landslides. In this study, 66 landslide locations, or 18.4 percent, were found in built-up land and 156 locations, or 43.5 percent, in cultivated and open land. Both types of land cover indicate the intervention of human activities. Meanwhile, only 136 landslide locations, or 37.9 percent, were found on non-cultivated land, including forest. According to [49], naturally vegetated areas such as forests can withstand shear stress soil due to strengthening by roots. Furthermore, it can reduce the chance of landslides. The study using the combination of NSBAS and superimposed lithological formation and slopes can identify the distribution of landslide locations. Most of the landslide locations are located on volcanic rocks and volcanic sediments with slopes of 15-30°. The frequency of landslide occurrences increases until the slope class of 15-20°, then decreases as the slope class increases.

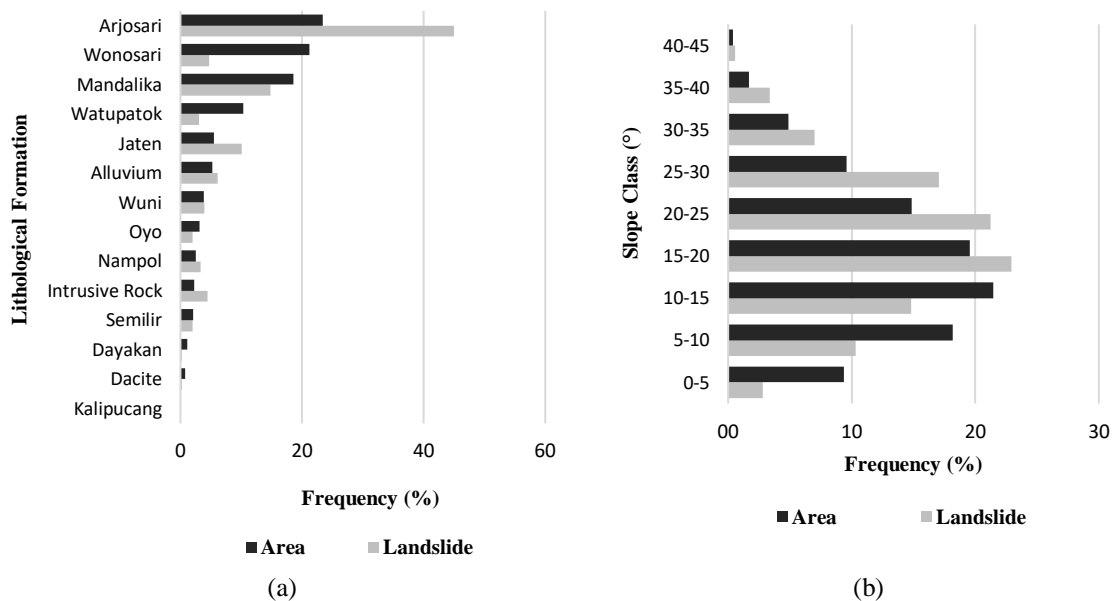


Figure 8. Frequency distribution of landslide in each (a) lithological formation and (b) slope class

3.3. The advantages and limitations of using LiCSBAS module

Sentinel-1 SAR data processing using LiCSBAS has several advantages. First, LiCSBAS can be a solution for mapping and assessing surface deformation velocity over a large area [19]. Second, the critical Sentinel-1 SAR data is accessible and already processed by LiCSAR [19], [20]. Third, users can freely access LiCSAR products through the COMET-LiCS website without downloading large datasets to their computers [19], [20]. The utilization of LiCSAR data can reduce processing time and memory usage. In addition, the use of Sentinel-1 SAR data allows temporal analysis possible every six days in the study area. Utilization of the NSBAS method in the LiCSBAS module can reduce the gap and the de-correlation between time in the network [19], [34]. On the other hand, LiCSBAS has limited utilization because it relies on sufficient LiCSAR data [19], [20].

However, some limitations have become essential matters. In this study, multi-temporal InSAR processing using LiCSBAS succeeded in detecting surface deformation at 100 landslide locations out of a total

of 358 landslide locations. The 100 landslide locations, on average, have an area of more than 1 hectare with an open landslide area without vegetation cover. The 100 landslide locations, on average, have an area of more than 1 hectare with an open landslide area without vegetation cover. This condition is related to the LiCSBAS output deformation pixels of 100 meters [19]. In addition, LiCSBAS utilizes LiCSAR products derived from Sentinel-1 with C-band [19], [20]. In densely vegetated areas, the Sentinel-1 C-band data produces interferograms with low coherence. LiCSBAS will automatically eliminate interferogram pixels with coherence values of less than 0.5. Some researchers have shown that C-band data is more suitable for measuring surface deformation in urban areas [19], [20], [50]. In addition, the hilly morphology in the research area can cause errors such as shadows. However, the combination of the LiCSBAS module and overlay of lithological formation and slopes in the Pacitan study area succeeded in identifying surface deformation at 100 landslide locations.

4. CONCLUSION

This study presents the use of LiCSBAS, an open-source analysis module integrated with LiCSAR, as a novel approach to address the issue of surface deformation in landslide locations with various physical and environmental conditions. They are not in an urban area or a large area; instead, they are in the Pacitan Regency. In addition, landslide distribution was spatially mapped based on lithological formations and slope classes and the effect of vegetation cover dynamics, using superimposed and Leaf Area Index analysis.

Based on the results of the overlay analysis, 280 locations of landslides, or 73.5 percent, occurred in volcanic rocks and volcanic sediments, especially from the Arjosari, Mandalika, and Jaten formations, which form steep slopes and are prone to landslide – these rock types are spread throughout the district, except in the western part. Meanwhile, as many as 219 landslide locations, or 61 percent, are in the 15-30° slope class. The frequency of landslide locations increases until the slope class is 15-30°, then decreases with increasing slope value.

ACKNOWLEDGEMENTS

We are grateful to the Ministry of Research and Technology/National Research and Innovation Agency for support and research funding grant number NKB-469/UN2.RST/HKP.05.00/202 through *Insinas* (National Innovation System Incentive). We also thank members of the Department of Geography, Universitas Indonesia, for their encouragement. LiCSAR contains modified Copernicus Sentinel data 2017-2020 analyzed by the Centre for the Observation and Modelling of Earthquakes, Volcanoes and Tectonics (COMET). LiCSAR uses JASMIN, the UK's collaborative data analysis environment (<http://jasmin.ac.uk>).

REFERENCES




- [1] Y. G. Yan, H. Y. Dai, L. L. Ge, J. T. Guo, A. H. M. Ng, and X. J. Li, "Numerical simulation of dynamic surface deformation based on DInSAR monitoring," *Transactions of Nonferrous Metals Society of China (English Edition)*, vol. 24, no. 4, pp. 1248–1254, 2014, doi: 10.1016/S1003-6326(14)63186-1.
- [2] B. H. Martins, M. Suzuki, P. E. Yastika, and N. Shimizu, "Ground surface deformation detection in complex landslide area—bobonaro, timor-leste—using SBAS DinSAR, UAV photogrammetry, and field observations," *Geosciences (Switzerland)*, vol. 10, no. 6, pp. 1–26, 2020, doi: 10.3390/geosciences10060245.
- [3] WP/WLI and UNESCO, *Multilingual Landslide Glossary*. Richmond: BiTech Publisher, 1993.
- [4] V. Vakhshoori, H. R. Pourghasemi, M. Zare, and T. Blaschke, "Landslide susceptibility mapping using GIS-based data mining algorithms," *Water (Switzerland)*, vol. 11, no. 11, pp. 7–13, 2019, doi: 10.3390/w11112292.
- [5] Regency Office of Pacitan, "Disaster in Pacitan Damaged 615 Residents Houses and 23 Kilometers of Roads," *pacitankab.go.id*, 2017. <https://pacitankab.go.id/bencana-pacitan-rusak-615-rumah-warga-dan-23-ribu-meter-jalan/> (accessed Nov. 18, 2020).
- [6] S. Bianchini, F. Cigna, C. Del Ventisette, S. Moretti, and N. Casagli, "Detecting and monitoring landslide phenomena with TerraSAR-X persistent scatterers data: The Gimigliano case study in Calabria Region (Italy)," *2012 IEEE International Geoscience and Remote Sensing Symposium*, pp. 982–985, 2012, doi: 10.1109/IGARSS.2012.6351237.
- [7] H. R. Pourghasemi and M. Rossi, "Landslide susceptibility modeling in a landslide prone area in Mazandarn Province, north of Iran: a comparison between GLM, GAM, MARS, and M-AHP methods," *Theoretical and Applied Climatology*, vol. 130, no. 1–2, pp. 609–633, 2016, doi: 10.1007/s00704-016-1919-2.
- [8] T. Strozzi *et al.*, "Satellite SAR interferometry for the improved assessment of the state of activity of landslides: A case study from the Cordilleras of Peru," *Remote Sensing of Environment*, vol. 217, no. January, pp. 111–125, 2018, doi: 10.1016/j.rse.2018.08.014.
- [9] G. Aslan, M. Fomelis, D. Raucoules, M. De Michele, S. Bernardie, and Z. Cakir, "Landslide mapping and monitoring using persistent scatterer interferometry (PSI) technique in the French alps," *Remote Sensing*, vol. 12, no. 8, 2020, doi: 10.3390/RS12081305.
- [10] A. Ferretti, C. Prati, and F. Rocca, "Permanent scatterers in SAR interferometry," *IEEE Transactions on Geoscience and Remote Sensing*, vol. 39, no. 1, pp. 8–20, 2001, doi: 10.1109/36.898661.
- [11] X. Hu *et al.*, "Timer-series InSAR analysis of cascade landslide complex, Washington, USA," *International Geoscience and Remote Sensing Symposium (IGARSS)*, no. December 2017, pp. 5093–5096, 2017, doi: 10.1109/IGARSS.2017.8128148.
- [12] G. Cianflone, C. Tolomei, C. A. Brunori, S. Monna, and R. Dominici, "Landslides and subsidence assessment in the Crati Valley

- (Southern Italy) using insar data,” *Geosciences (Switzerland)*, vol. 8, no. 2, 2018, doi: 10.3390/geosciences8020067.
- [13] Y. Yan and Y. Wang, “Impact of the variation of observable areas on landslide study using InSAR technique,” *International Geoscience and Remote Sensing Symposium (IGARSS)*, no. June 2017, pp. 9606–9609, 2019, doi: 10.1109/IGARSS.2019.8899071.
- [14] M. B. Kursah and Y. Wang, “Small baseline subset Interferometric SAR technique for spatiotemporal analysis of the recent landslides, Sierra Leone,” *2019 IEEE International Geoscience and Remote Sensing Symposium*, pp. 1986–1989, 2019, doi: 10.1109/IGARSS.2019.8899096.
- [15] D. Meghanadh, A. Tiwari, and R. Dwivedi, “Multicriteria analysis for landslide inventory mapping using PS-InSAR,” *Proceedings of the 2019 IEEE Recent Advances in Geoscience and Remote Sensing: Technologies, Standards and Applications, TENGARSS 2019*, pp. 30–33, 2019, doi: 10.1109/TENGARSS48957.2019.8976054.
- [16] A. Singh Virk, A. Singh, and S. K. Mittal, “Advanced MT-InSAR landslide monitoring: methods and trends,” *Journal of Remote Sensing & GIS*, vol. 07, no. 01, pp. 1–6, 2018, doi: 10.4172/2469-4134.1000225.
- [17] S. Mirzaee, M. Motagh, B. Akbari, H. U. Wetzel, and S. Roessner, “Evaluating three InSAR time-series methods to assess creep motion, case study: Masouleh landslide in North Iran,” *ISPRS Annals of the Photogrammetry, Remote Sensing and Spatial Information Sciences*, vol. 4, no. 1W1, pp. 223–228, 2017, doi: 10.5194/isprs-annals-IV-1-W1-223-2017.
- [18] Z. Zeng, Y. Wang, Y. Yan, N. Xiao, and D. Chen, “Analyzing landslide-prone loess area of Heifangtai, Gansu, China using SBAS-InSAR technique,” in *IGARSS 2018 - 2018 IEEE International Geoscience and Remote Sensing Symposium*, 2018, pp. 4889–4892, doi: 10.1109/IGARSS.2018.8518328.
- [19] Y. Morishita, M. Lazecky, T. J. Wright, J. R. Weiss, J. R. Elliott, and A. Hooper, “LiCSBAS: An open-source insar time series analysis package integrated with the LiCSAR automated sentinel-1 InSAR processor,” *Remote Sensing*, vol. 12, no. 3, pp. 5–8, 2020, doi: 10.3390/rs12030424.
- [20] M. Lazecký *et al.*, “LiCSAR: an automatic InSAR tool for measuring and monitoring tectonic and volcanic activity,” *Remote Sensing*, vol. 12, no. 15, 2020, doi: 10.3390/rs12152430.
- [21] Y. Morishita, “Nationwide urban ground deformation monitoring in Japan using Sentinel-1 LiCSAR products and LiCSBAS,” *Progress in Earth and Planetary Science*, vol. 8, no. 1, 2021, doi: 10.1186/s40645-020-00402-7.
- [22] BPS-Statistics of Pacitan Regency, “Pacitan Regency in figures 2020,” *BPS-Statistics of Pacitan Regency*, 2020. <https://pacitankab.bps.go.id/publication/2020/04/27/59b932e91b04de081ce4c48f/kabupaten-pacitan-dalam-angka-2020.html> (accessed Dec. 28, 2020).
- [23] Geospatial Information Agency, “Digital topographic map of Indonesia,” *Peta RBI Indonesia*, 2016. <https://tanahair.indonesia.go.id/portal-web/> (accessed Dec. 25, 2020).
- [24] R. W. van Bemmelen, *The Geology of Indonesia*, vol. 1A. The Hague, 1949.
- [25] Geospatial Information Agency, “Digital elevation model National (DEMNAS),” *Digital Elevation Model Nasional-DEMNAS*, 2018. <https://tanahair.indonesia.go.id/demnas/#/> (accessed Dec. 25, 2020).
- [26] L. Jacobs *et al.*, “Landslide characteristics and spatial distribution in the Rwenzori Mountains, Uganda,” *Journal of African Earth Sciences*, vol. 134, pp. 917–930, 2017, doi: 10.1016/j.jafrearsci.2016.05.013.
- [27] G. P. Asner, J. M. O. Scurlock, and J. A. Hicke, “Global synthesis of leaf area index observations: implications for ecological and remote sensing studies,” *Global Ecology & Biogeography*, vol. 12, pp. 191–205, 2003, doi: 10.1046/j.1466-822X.2003.00026.x.
- [28] E. Boegh *et al.*, “Airborne multispectral data for quantifying leaf area index, nitrogen concentration, and photosynthetic efficiency in agriculture,” *Remote Sensing of Environment*, vol. 81, no. 2–3, pp. 179–193, 2002, doi: 10.1016/S0034-4257(01)00342-X.
- [29] H. Samodra, S. Gafoer, and Tjokrosapoetro, “Geological map of the Pacitan Quadrangle, Java,” *Geological Research and Development Centre, Bandung*. Bandung, 1992.
- [30] Sampurno and H. Samodra, “Geological map of the Ponorogo Quadrangle, Java.” Bandung, 1997.
- [31] European Space Agency, “Sentinel 2 Imagery,” *Copernicus Sentinel Data*, 2020. <https://scihub.copernicus.eu/dhus/#/home> (accessed Dec. 28, 2020).
- [32] J. Biggs, T. Wright, Z. Lu, and B. Parsons, “Multi-interferogram method for measuring interseismic deformation: Denali Fault, Alaska,” *Geophysical Journal International*, vol. 170, no. 3, pp. 1165–1179, 2007, doi: 10.1111/j.1365-246X.2007.03415.x.
- [33] J. P. Galve *et al.*, “Evaluation of the SBAS InSAR service of the European space Agency’s Geohazard Exploitation Platform (GEP),” *Remote Sensing*, vol. 9, no. 12, 2017, doi: 10.3390/rs9121291.
- [34] P. López-Quiroz, M. P. Doin, F. Tupin, P. Briole, and J. M. Nicolas, “Time series analysis of Mexico City subsidence constrained by radar interferometry,” *Journal of Applied Geophysics*, vol. 69, no. 1, pp. 1–15, 2009, doi: 10.1016/j.jappgeo.2009.02.006.
- [35] X. Chen, Q. Sun, and J. Hu, “Generation of complete SAR geometric distortion maps based on DEM and neighbor gradient algorithm,” *Applied Sciences (Switzerland)*, vol. 10, no. 11, pp. 1–14, 2018, doi: 10.3390/app8112206.
- [36] R. Ramirez, S. R. Lee, and T. H. Kwon, “Long-term remote monitoring of ground deformation using sentinel-1 interferometric synthetic aperture radar (INSAR): Applications and insights into geotechnical engineering practices,” *Applied Sciences (Switzerland)*, vol. 10, no. 21, pp. 1–20, 2020, doi: 10.3390/app10217447.
- [37] K. Nikolakopoulos *et al.*, “Preliminary results from active landslide monitoring using multidisciplinary surveys,” *European Journal of Remote Sensing*, vol. 50, no. 1, pp. 280–299, 2017, doi: 10.1080/22797254.2017.1324741.
- [38] K. Shirani and M. Pasandi, “Detecting and monitoring of landslides using persistent scattering synthetic aperture radar interferometry,” *Environmental Earth Sciences*, vol. 78, no. 1, pp. 1–24, 2019, doi: 10.1007/s12665-018-8042-x.
- [39] School of Earth and Environment The University of Leeds, “COMET-LiCS Sentinel-1 InSAR Portal,” *LiCSAR Products*. 2013.
- [40] G. Samodra, N. Ngadisih, M. N. Malawani, D. Mardiatno, A. Cahyadi, and F. S. Nugroho, “Frequency–magnitude of landslides affected by the 27–29 November 2017 Tropical Cyclone Cempaka in Pacitan, East Java,” *Journal of Mountain Science*, vol. 17, no. 4, pp. 773–786, 2020, doi: 10.1007/s11629-019-5734-y.
- [41] O. F. Althuwaynee, B. Pradhan, and S. Lee, “Application of an evidential belief function model in landslide susceptibility mapping,” *Computers and Geosciences*, vol. 44, pp. 120–135, 2012, doi: 10.1016/j.cageo.2012.03.003.
- [42] E. Haryono and M. Day, “Landform differentiation within the Gunung Kidul Kegelkarst, Java, Indonesia,” *Journal of Cave and Karst Studies*, vol. 66, no. 2, pp. 62–69, 2004.
- [43] C. W. Chen, H. Saito, and T. Oguchi, “Rainfall intensity–duration conditions for mass movements in Taiwan,” *Progress in Earth and Planetary Science*, vol. 2, no. 1, 2015, doi: 10.1186/s40645-015-0049-2.
- [44] W. Chen, H. R. Pourghasemi, A. Kornejady, and N. Zhang, “Landslide spatial modeling: Introducing new ensembles of ANN, MaxEnt, and SVM machine learning techniques,” *Geoderma*, vol. 305, no. May, pp. 314–327, 2017, doi: 10.1016/j.geoderma.2017.06.020.
- [45] S. Çellek, “Effect of the slope angle and its classification on landslide,” *Natural Hazards and Earth System Sciences Discussions*, no. May, pp. 1–23, 2020, doi: 10.5194/nhess-2020-87.
- [46] P. Xie, A. Zhou, and B. Chai, “The application of long short-term memory (LSTM) method on displacement prediction of multifactor-induced landslides,” *IEEE Access*, vol. 7, pp. 54305–54311, 2019, doi: 10.1109/ACCESS.2019.2912419.




- [47] J. W. Godt, R. L. Baum, and N. Lu, "Landsliding in partially saturated materials," *Geophysical Research Letters*, vol. 36, no. 2, pp. 1–5, 2009, doi: 10.1029/2008GL035996.
- [48] D. T. Bui, O. Lofman, I. Revhaug, and O. Dick, "Landslide susceptibility analysis in the Hoa Binh province of Vietnam using statistical index and logistic regression," *Natural Hazards*, vol. 59, no. 3, pp. 1413–1444, 2011, doi: 10.1007/s11069-011-9844-2.
- [49] B. Feby, A. L. Achu, K. Jimnisha, V. A. Ayisha, and R. Reghunath, "Landslide susceptibility modelling using integrated evidential belief function based logistic regression method: A study from Southern Western Ghats, India," *Remote Sensing Applications: Society and Environment*, vol. 20, no. August, 2020, doi: 10.1016/j.rsase.2020.100411.
- [50] K. Zhou, F. Wang, M. Wang, and Q. Ding, "Land surface deformation monitoring of the songyuan langya dam using mt-InSAR," *IEEE Transactions on Geoscience and Remote Sensing*, no. 2001, pp. 2019–2022, 2019, doi: 10.1109/BIGSARDATA.2019.8858452.

BIOGRAPHIES OF AUTHORS






Dimas Bayu Ichsandya    is a student at the Department of Geography, Faculty of Mathematics and Natural Sciences, Universitas Indonesia, where he is pursuing a degree in Bachelor of Science. His research interest is focusing on remote sensing and natural hazard susceptibility mapping using the Geographic Information System. He can be contacted at email: dimas.bayu72@ui.ac.id.






Muhammad Dimiyati    was born in Solo. He obtained his BSc (1982) from the Faculty of Geography, Department of Remote Sensing, Gadjah Mada University, and Master (1990) and Doctoral Degree (1997) of Agricultural Science, Lab of Regional Planning, Tropical Agriculture Division, Faculty of Agriculture, Kyoto University, Japan. Since 1983-2005, he has been working for the Ministry of Public Works in Remote Sensing, Geographic Information Systems, and Spatial Planning. He was the Deputy Assistant of Large-Scale Area Development, then Deputy Assistant of Integrated Infrastructure, Deputy Assistant of Cooperation and Partnerships, and Deputy Assistant of Formal Housing Planning of the Ministry of Housings (2005-2014). He was the Deputy of Resources for Science and Technology of the Ministry of Science and Technology (2014-2015). He was a Director General of Strengthening for Research and Development, Ministry of Research, Technology, and Higher Education (2015-2020). Currently, he is an Associate Professor in the Department of Geography, Faculty of Natural Sciences and Mathematics, Universitas Indonesia. He can be contacted at email: m.dimiyati@sci.ui.ac.id.






Iqbal Putut Ash Shidiq    was born in Jakarta. He currently enrolls as a Ph.D. student in the Faculty of Forestry and Environment, Universiti Putra Malaysia, majoring in remote sensing for forest carbon and biomass analysis. He received his S.Si. (Sarjana Sains or Bachelor of Science) from Universitas Indonesia (2008) in Geography. In 2012 he obtained his M.Sc. in Geo-information for Spatial Planning and Risk Management from Gadjah Mada University of Yogyakarta. Besides work as a post-graduate student, he also has served as lecturer and researcher staff in the Laboratory of GIS, Department of Geography, Universitas Indonesia, since 2016. He has published several papers in indexed journals and -proceedings during his working time. In addition, he has followed various researches and works that are mainly related to GIS and remote sensing subjects. He also acts both as a participant and trainer in several workshops. His interest is in developing GIS and remote sensing applications, disaster risk management, and land surveying. He can be contacted at email: iqbalputut@sci.ui.ac.id.






Faris Zulkarnain    was born in Jakarta. He obtained his Bachelor of Science (2013) from the Department of Geography, Faculty of Mathematics and Natural Science, Universitas Indonesia, and his Master of Engineering (2017) from the Department of Civil Engineering, Faculty of Engineering, Universitas Indonesia. Currently, he is a lecturer in the Department of Geography, Faculty of Mathematics and Natural Sciences, Universitas Indonesia. His research interest is in water resources management, Geographic Information systems, remote sensing, and urban environment. He can be contacted at email: faris.zulkarnain@sci.ui.ac.id.






Nurul Sri Rahatiningtyas    was born in Jakarta. She obtained her BSc (2005) from the Department of Geography Faculty of Mathematics and Natural Sciences Universitas Indonesia. And Master (2011) in Marine and Coastal Resources Management from IPB University Indonesia. Currently (since 2012), she is working as a Lecturer in the Department of Geography, Faculty of Mathematics and Natural Sciences, Universitas Indonesia. She is also working as a researcher in the Center for Applied Geography Research Faculty of Mathematics and Natural Sciences Universitas Indonesia (since 2012 – now) and Disaster Risk Reduction Center Universitas Indonesia (since 2017 – now). Since 2018, She is a member of U-INSPIRE Indonesia (a platform of Youth and Young Professionals working in Science, Engineering, Technology, and Innovation (SETI) for Disaster Risk Disasters (DRR)). In addition, she was the PIC of Knowledge Management Working Group U-INSPIRE Indonesia (2019-2021). Moreover, since 2019 She has been a member of the U-INSPIRE Alliance. She can be contacted at email: nurul.sr@ui.ac.id.



Riza Putera    was born in Bandung. He obtained his Bachelor of Science (2014) from the Department of Geography, Faculty of Mathematics and Natural Science, Universitas Indonesia, and his Master of Urban Development Studies (2019) from the School of Strategic and Global Studies, Universitas Indonesia. Currently, he is a lecturer in the Department of Geography, Faculty of Mathematics and Natural Sciences, Universitas Indonesia. His research interest is in Geographic Information Systems, remote sensing, geomorphology, and spatial planning. He can be contacted at email: riza.putera@ui.ac.id.



Farhan Makarim Zein    was born in Bogor. He obtained his Bachelor of Science (2021) from the Department of Geography, Faculty of Mathematics and Natural Science, Universitas Indonesia. Currently, he is a research assistant in the Department of Geography, Faculty of Mathematics and Natural Sciences, Universitas Indonesia. His research interest is in land deformation detecting and mapping with Interferometric Synthetic Aperture Radar (InSAR). He can be contacted at email: farhan.makarim@ui.ac.id.